NATIONAL RADIO ASTRONOMY OBSERVATORY
Green Bank, West Virginia

Electronics Division Internal Report No. 57

CHARACTERISTICS OF THE PARABOLOIDAL
REFLECTOR ANTENNA

J. W. M. Baars

AUGUST 1966

CHARACTERISTICS OF THE PARABOLOIDAL REFLECTOR ANTENNA

J. W. M. Baars

Introduction

The literature on radio astronomy antennas, their theoretical characteristics and experimental evaluation is still rather scarce. But observers desire more and more an accurate knowledge of the parameters of the antenna which they use. Since greater accuracy of observations is required (variable sources) and more involved observing techniques come into application, a knowledge of instrumental character- istics is necessary.

Over the last three years we have tested most of the NRAO telescopes at several wavelengths. Results of these tests have been communicated in Electronics Division Internal Reports 30 (300-ft., 10 cm wavelength), 36 (85-ft., 2 cm), and a report on the 140-ft. (1, 2, and 6 cm) is forthcoming.

In connection with these tests, various theoretical problems of antennas were attacked in the hope to find explanations for the measured effects. These efforts resulted in formulae and curves, which sometimes have a wider applicability than just one antenna.

It is the aim of this report to bring together, without too much derivation and discussion, those results of our studies, which are of practical value for the evaluation of single aperture antennas and more specifically paraboloidal reflectors.

SPECIAL EMPHASIS IS LAID UPON PRESENTATION OF GRAPHS WHICH CAN BE USED DIRECTLY WITHOUT ADDITIONAL CALCULATIONS.

The following table lists the graphs collected at the end of this report. Also a list of symbols is given.

List of Figures

List of Symbols

A	antenna absorption area	β	maximum phase error caused by defocusing
A_g	antenna geometrical area	δ	$= d/D$, relative diameter of blocking area
$A(\rho)$	amplitude term of aperture field	ϵ	feed displacement from focal point
D	aperture diameter	η	efficiency
$F(\rho)$	aperture exitation function	θ	polar coordinate of farfield point
G	antenna gain	λ	wavelength
J_o	Bessel function of order zero	ρ	radial coordinate in aperture
R	distance from aperture along the axis	φ	azimuthal coordinate of farfield point
S	level (dB) of first sidelobe	φ	azimuthal coordinate in aperture plane
T	aperture field edge taper in dB	ψ_o	half angle of subreflector from feed
V	amplitude of first sidelobe	Θ	half power beamwidth (HPBW)
		Λ	lambda function
a	aperture radius	Φ	phase term of aperture field
	multiplicative constant in HPBW expression	Ψ_o	aperture angle of paraboloid
c	correlation length of random surface errors	Ω_A	antenna solid angle
d	diameter of blocking area	Ω_m	main beam solid angle.
$\bar{d}$	r.m.s. random surface error		
f	focal length of paraboloid		
g	farfield radiation pattern		
k	$= 2\pi/\lambda$, wavenumber		
m	Cassegrainian magnification factor		
n	exponent in aperture exitation function		
p	pedestal height of aperture field		
u	reduced polar coordinate of farfield point		

Summary of Aperture Theory

In this section we shall write down shortly the starting point for our calculations and the simplifying assumptions involved.

We consider the radiation pattern $g(\theta, \varphi)$ of a circular aperture antenna with an aperture exitation field (illumination function) $F(\rho, \varphi')$. We shall restrict ourselves mainly to pattern characteristics in the farfield (Fraunhofer region). The aperture field $F(\rho, \varphi')$ is assumed to be formed by reflection (using geometrical optics) of the radiation field of the feed. The feed is located in or near the focal point of the antenna reflector. We shall refer to the feed pattern as primary pattern, while $g(\theta, \varphi)$ is also called the secondary pattern. (See Figure 1 for the geometry.)

The secondary pattern is obtained by an integration of the aperture field over the area of the aperture. This is simply an application of the Huygens-Kirchhoff principle. The treatment is entirely in scalar form and the validity of the results is only warranted for large antennas (in terms of the wavelength, $D > 100\ \lambda$, say), farfield pattern and small angular region about the beam axis (few degrees). Then the secondary pattern is given by the integral

$$g(\theta, \varphi) = \int_0^a \int_0^{2\pi} F(\rho, \varphi') \exp\left[ik\,\rho \sin\theta \cos(\varphi - \varphi')\right] \rho\, d\rho\, d\varphi' \tag{1}$$

The aperture field $F(\rho, \varphi')$ can be written as

$$F(\rho, \varphi') = A(\rho, \varphi') \exp\left[i\,\Phi(\rho, \varphi')\right] \tag{2}$$

where $A(\rho, \varphi')$ is the amplitude and $\Phi(\rho, \varphi')$ the phase term.

In case of rotational symmetry and uniform phase in the aperture field, we can perform the integration in φ' to obtain

$$g(u) = 2\pi a^2 \int_0^1 A(\rho)\, J_0(u\rho)\, \rho\, d\rho \tag{3}$$

where moreover we have normalized to an aperture radius one and introduced the angular variable $u = ka \sin\theta$. $J_0(u\rho)$ is the Bessel function of order zero. For the

exitation function we choose

$$A(\rho) = p + (1 - p) (1 - \rho^2)^n, \quad 0 \leq p \leq 1, \quad n = 0, 1, 2, \ldots \tag{4}$$

the "hyperparabolic illumination on a pedestal" (p).

Integration of (3) after insertion of (4) gives

$$g(u) = \pi a^2 \left[p\Lambda_1(u) + (1 - p) \frac{\Lambda_{n+1}(u)}{n + 1} \right] \tag{5}$$

where $\Lambda_n(u) \equiv n! J_n(u) / \left(\frac{u}{2}\right)^n$ is the Lambda function. It is tabulated in Jahnke-Emde's Tables of Functions, p. 180ff.

For all our computations in the following we have used

$$A(\rho) = p + (1 - p) (1 - \rho^2) \tag{6}$$

the parabolic illumination on a pedestal. It gives a good approximation to the primary pattern of horn and dipole feeds. The radiation pattern becomes

$$g(u) = \pi a^2 \left[p\Lambda_1(u) + \frac{1 - p}{2} \Lambda_2(u) \right] \tag{7}$$

The taper T in dB of the aperture illumination is

$$T = 20 \log p \tag{8}$$

The effect of tapering the illumination function towards the edge of the aperture on the secondary pattern is:

    a. Lower efficiency (directivity, gain).

    b. Larger beamwidth.

    c. Lower sidelobes.

It is clear that a. and b. are not desirable, while c. is. The adjustment of the taper makes a compromise between incompatible requirements possible.

Basic Antenna Parameters

The important parameters of an antenna are:

Beamwidth to half power points (HPBW).

Directivity or gain (G).

Aperture efficiency ($\eta_A = A/A_g$).

Main beam efficiency (η_B).

Level of the first sidelobe (S).

Spillover radiation and cross polarization level.

Formulae interrelating some of these parameters are:

$$G = \frac{4\pi}{\lambda^2} A = \frac{4\pi}{\Omega_A} = \frac{4\pi}{\Omega_m} \eta_B \tag{9}$$

$$\eta_A = \frac{\lambda^2}{\Omega_m A_g} \eta_B \approx 0.76 \, \eta_B \tag{10}$$

where the factor 0.76 is valid for NRAO telescopes. It assumes an edge taper of -18 dB and a HPBW $\Theta_A = 4200 \, \lambda/D$ (in arc-minutes). A two-dimensional gaussian curve is an excellent approximation of the main beam. Then we have for the main beam solid angle

$$\Omega_m = 1.133 \, \Theta_A^2 \tag{11}$$

We shall now give some graphs interrelating the parameters. Because the graphs mainly speak for themselves, only short comments will be given in the text.

Figure 2 shows the relations between taper T, pedestal height p, sidelobe level S and sidelobe amplitude V. Using this set one can easily find the necessary edge taper for a desired sidelobe level, etc. The two scales pertaining to a particular curve are indicated by bars around the curve designation. We shall use the graph as an auxiliary later on.

In Figure 3 the relative efficiency and the HPBW are given as a function of illumination edge taper. From this figure one can read directly how much the aperture efficiency has decreased from the value with uniform illumination and also the percentage beam broadening when the illumination is tapered. The high efficiencies are not obtained in practice because of aperture blocking by front-end box and support legs, feed losses, spillover radiation. A maximum of 0.6-0.7 is typical for -18 dB taper.

Deviations from the Ideal Situation

Up to now we have dealt with an ideal circular aperture reflector and its radiation field. In practice, however, several deviations from this ideal situation exist. These are:

1. Random deviations of the reflector contour from a perfect paraboloid.

2. Obscuration of a part of the reflector by front-end box, Cassegrainian subreflector and support legs.

3. Axial and/or lateral displacement of the feed from the focal point.

These cause changes in the aperture field $A(\rho, \varphi')$ and hence in the secondary pattern characteristics. We shall now show the effect of each of these perturbations.

1. Random deviations of the reflector surface introduce a random phase variation over the aperture plane of $\Delta\Phi = 4\pi\bar{d}/\lambda$, where $\bar{d}$ is the rms deviation from the perfect paraboloid. The aperture efficiency dependence on the rms surface errors is given by the formula (Ruze):

$$\eta_A = \eta_{A_o} \exp\left[-\left(\frac{4\pi\bar{d}}{\lambda}\right)^2\right] \tag{12}$$

This formula is valid if the correlation length c of the surface errors is much smaller than the wavelength; this is a normal situation with radio telescopes. Figure 4 is a set of curves which shows the maximum usable frequency for a certain efficiency loss as a function of the rms surface error $\bar{d}$.

It is by now standard procedure to measure the aperture efficiency of an antenna at several wavelengths and to plot $\ell n \, (\eta_A/\eta_{A_0})$ against $1/\lambda^2$. The slope of the straight line through the points gives $\bar{d}$.

The surface errors give rise to a so-called scatter- or error-pattern. Its width and level are determined by the correlation length c and the surface error $\bar{d}$. If the mean square phase error $\Delta\Phi^2 \lesssim 1$, we have for the width Θ_s of the scatter pattern

$$\Theta_s \approx \frac{D}{c} \, \Theta_A \tag{13}$$

The axial gain of the scatter pattern increases with increasing correlation length and increasing surface error. This is depicted in Figure 5, where the dependence of the aperture efficiency/ (on linear and dB scale) and the scatter pattern level G_s, with respect to the main beam axial gain G_m, on the surface error is given. The curves of the scatter pattern gain for other correlation intervals run parallel to the one given. The crosses indicate the levels of these lines at $\bar{d}/\lambda = 0.54$.

2. Feed and front-end box or subreflector (in a Cassegrain) with their support legs block a certain part of the reflector for the incoming radiation. I have analyzed the case where the central circular part of the aperture (up to a diameter d) is obscured. The result of the calculations for gain decrease and sidelobe level is given in Figures 6 and 7. The full line is the exact behavior; the dashed lines are found from the approximation formula

$$S = 20 \log \left[\frac{V + \dfrac{2}{1+p} \, \delta^2}{1 - \dfrac{2}{1+p} \, \delta^2} \right] \tag{14}$$

where $\delta = d/D$. In applying this formula, good use can be made of Figure 2.

The results for 18 dB taper lie very close to the curves for parabolic illumination. A very simple formula for the increase of the sidelobe level is

$$\Delta S = (82 + 10.25 \, T) \, \delta^2 \, (dB) \tag{15}$$

It is good to within 1 dB for values $\delta \lesssim 0.15$ and taper $9 \lesssim T \lesssim 18 \, (dB)$.

The HPBW of an annular aperture is smaller than that of the full aperture with the same outer diameter. Figure 8 shows the relative decrease in HPBW as a function of the blocking parameter for uniform and parabolic illumination.

3. Whenever the phase center of the feed is not located in the focal point of the antenna, the gain will be lower, the sidelobe level higher and the beamwidth larger. We can resolve an arbitrary feed displacement in a component along the axis of symmetry (axial defocusing) and perpendicular to it (lateral defocusing). The total gain decrease in dB due to an arbitrary defocusing is the sum of the gain loss of the off-axis beam without axial defocusing (purely lateral feed displacement) and the gain loss of an axially defocused on-axis beam.

a. Axial defocusing. The displacement ϵ_a along the axis causes a phase error β_a over the aperture in even powers of the radial coordinate ρ. The decrease in gain depends on the illumination taper. For uniform illumination it is

$$G/G_0 = \left[\frac{\sin(\beta_a/2)}{\beta_a/2} \right]^2 \approx 1 - \beta_a^2/12 \tag{16}$$

and for parabolic illumination

$$G/G_0 = \left[\frac{\sin(\beta_a/2)}{\beta_a/2} \right]^4 + \frac{4}{\beta_a^2} \left[\frac{\sin\beta_a}{\beta_a} - 1 \right]^2 \approx 1 - \beta_a^2/18 \tag{17}$$

where $\beta_a = \frac{2\pi}{\lambda} \epsilon_a (1 - \cos\Psi_0)$ is the phase error at the rim of the reflector; Ψ_0 is the aperture angle. (See Figure 1.)

Figure 9 is a plot of equations (16) and (17); the dashed lines are the quadratic approximations. The sidelobe level S is also given. The beam broadening has been calculated and is shown in Figure 10. The experimentally determined beam broadening at 2 cm wavelength at the 85-ft. and 140-ft. is inserted. The same formulae (16) and (17) hold for the gain variation with axial defocusing in the case of an off-axis beam, i.e., where lateral defocusing is also present.

   b. Lateral defocusing is connected with a phase error over the aperture in odd powers of ρ. Consequently it causes a beam tilt, which is in opposite direction to the feed displacement. The angular beam tilt is somewhat smaller than the angular feed displacement, because the reflecting surface is not flat. The connecting factor is the beam deviation factor (BDF), which of course is strongly dependent on the F/D ratio. Figure 11 shows the BDF as a function of the F/D ratio of the reflector for three illumination functions. The dependence on illumination taper is given in Figure 12 for an F/D = 0.425 (NRAO telescopes).

   The effect on the gain is much less than with axial feed displacement, but the increase of the sidelobe level at the side of the antenna axis is very strong. This sidelobe is called the coma lobe. Figure 13 shows the gain decrease and the coma lobe level for several values of the taper. The scale at the right is in percent of the axial gain. The curves apply to a F/D = 0.425. The sidelobe level dependence on beam tilt for a typical Cassegrain (F/D = 4) is also given. The increase in beamwidth is small, less than 2 percent for 4 HPBW off-axis.

   If we write the HPBW as $\Theta_A = b\lambda/D$ (radian), we have for the feed displacement ϵ_ℓ per HPBW beam tilt

$$\epsilon_\ell / \text{HPBW} = \frac{b}{\text{BDF}} \frac{F}{D} \lambda \tag{18}$$

The factor b depends on the illumination taper. (See Figure 3.) The BDF depends on both taper and F/D ratio (Figures 11 and 12). For the NRAO telescopes with F/D = 0.425 and taper T = -18 dB, we find

$$\epsilon_\ell / \text{HPBW} = 0.6 \lambda$$

For the 36-ft. antenna with F/D = 0.8 and the same taper we obtain

$$\epsilon_\ell / \text{HPBW} = 1.0 \lambda .$$

Cassegrainian Antennas

As is well known, a Cassegrain with a magnification m is equivalent to a prime focus instrument with m times the F/D ratio of the primary paraboloid. For all Cassegrains the BDF can be taken as one.

The coma lobe effect is very much less serious for large F/D ratios as is apparent from the bottom curves of Figure 13. These were calculated for $(F/D)_{eff}$ = 4.0; the results, however, are about the same for $2.5 \leq (F/D)_{eff} \leq 6$. The feed displacement needed for one HPBW beam tilt is m times the one required in a prime focus with the same F/D ratio for the paraboloid.

The influence of axial feed displacement on the gain is very small. An axial movement of the secondary reflector, however, has an even stronger effect than the feed in the primary focus. The largest phase error (at the edge of the aperture) β_a is connected to a displacement ϵ_a by the formulae:

Feed displacement: $\qquad \beta_a = \dfrac{2\pi}{\lambda} \, \epsilon_a \, (1 - \cos \psi_0)$ $\qquad\qquad\qquad$ (19)

Secondary reflector: $\qquad \beta_a = \dfrac{2\pi}{\lambda} \, \epsilon_a \left[(1 - \cos \Psi_0) + (1 - \cos \psi_0) \right]$ $\qquad\quad$ (20)

Here Ψ_0 is the aperture angle of the paraboloid (Figure 1) and $2\psi_0$ is the angle under which the subreflector is seen from the feed (secondary focus). These should be compared with the formula following equation (17) for the feed movement in the primary focus.

It is clear that the feed position in a Cassegrain is not critical at all. This is an advantage if receiver front-end changes are being made frequently.

Atmospheric Influences

With modern low-noise radiometers and much interest in the high frequency region of the spectrum (above 3 GHz) it has become clear that often the atmosphere (troposphere) determines the sensitivity limit of the radio telescope. Especially the fluctuations in the thermal radiation of the atmospheric constituents offer severe difficulties at wavelengths below 6 cm and cause that observations have to be confined to clear days with stable weather.

The "dual beam" (or "switched beams") technique has been tested quite exten-
sively at 9. 5 mm, 2 and 6 cm with the 140-ft. It causes a dramatic decrease in
atmospheric noise fluctuations. Typical is a factor 10-20 at 2 cm in light rain or
with cloudy sky. The effect of the method depends of course on the separation of the
two beams. Figure 14 shows the percentage of power flowing in a region of space
common to both beams as a function of the distance to the antenna. In using this graph
one can take into account that the bulk of the atmospheric fluctuations occur in the
lowest 2-3 kilometers of the troposphere. The effect of the method is often better than
predicted by Figure 14, because the atmospheric fluctuations are correlated over
certain distances. Thus partly overlapping beams still produce a noticable reduction.

The beams generally are completely separated at a distance about equal to the
Rayleigh distance R_r, which is defined as $R_r = D^2/2\lambda$. In Figure 15 we give the
Rayleigh distance as a function of the wavelength for antennas of 11, 26, 43, and 92
meter diameter (36, 85, 140, and 300 feet, respectively). The farfield distance, i.e.,
the minimum distance at which farfield pattern characteristics can be measured, is
per definition 4 times the Rayleigh distance: $R_f = 4R_r = 2D^2/\lambda$.

As an example of the efficiency of the dual beam method Figure 16 is included
in this report. It shows recordings of the sky brightness with the antenna directed
towards the zenith. The single beam (SB) and dual beam (DB) observation of 20 minutes
duration each were recorded directly after each other under similar weather conditions.
The vertical scale is in antenna temperature. It is evident that the DB mode gives
smaller noise fluctuations and a more stable baseline. The records are typical,
certainly not an extreme. At 2 cm wavelength we have measured frequently variations
in excess of 15 °K during rain; on the other hand, sometimes in clear and dry weather
the difference between the two modes is marginal.

For frequencies above 3 GHz the atmospheric attenuation becomes a factor of
importance. Especially in the millimeter wavelength range the absorption bands of
water vapor and oxygen cause such high values of the attenuation that observations
have to be confined to rather narrow frequency "windows". The attenuation is of
course strongly dependent on the total amount of water vapor in the line of sight.
Several curves can be found in R. Menon's Internal NRAO Report, January 1964.

Acknowledgement

It is with pleasure that I mention Peter Mezger, under whose guidance many of the telescope measurements were performed and who provided ample encouragement for the theoretical work.

References

"Theory of Aperture Antennas and Paraboloidal Reflector", S. Silver, Microwave Antenna Theory and Design, Chapters 6 and 12.

"A Comparison Between Prime Focus and Cassegrain Antennas", J. W. M. Baars, NRAO Internal Report, October 1964.

NRAO Telescopes:
J. W. M. Baars and P. G. Mezger, "The Characteristics of the 300-Foot Telescope at 10 Centimeter Wavelength", Electronics Division Internal Report No. 30, May 1964.

J. W. M. Baars and P. G. Mezger, "The Characteristics of the NRAO 85-Foot Telescopes at 2 cm Wavelength", Electronics Division Internal Report No. 36, October 1964.

P. G. Mezger and many others, "Radio Tests of the NRAO 140-Foot Telescope in the Wavelength Range Between 0.95 and 11 Centimeters"; forthcoming report.

Dual Beam Observing Technique:
R. G. Conway, Nature 199 (1963), No. 4899, 1177.
J. W. M. Baars, Nature, submitted.
Rama C. Menon, "Atmospheric Absorption in the Range of Wavelength Between 10 cm and 1 Micron", NRAO Internal Report, January 1964.
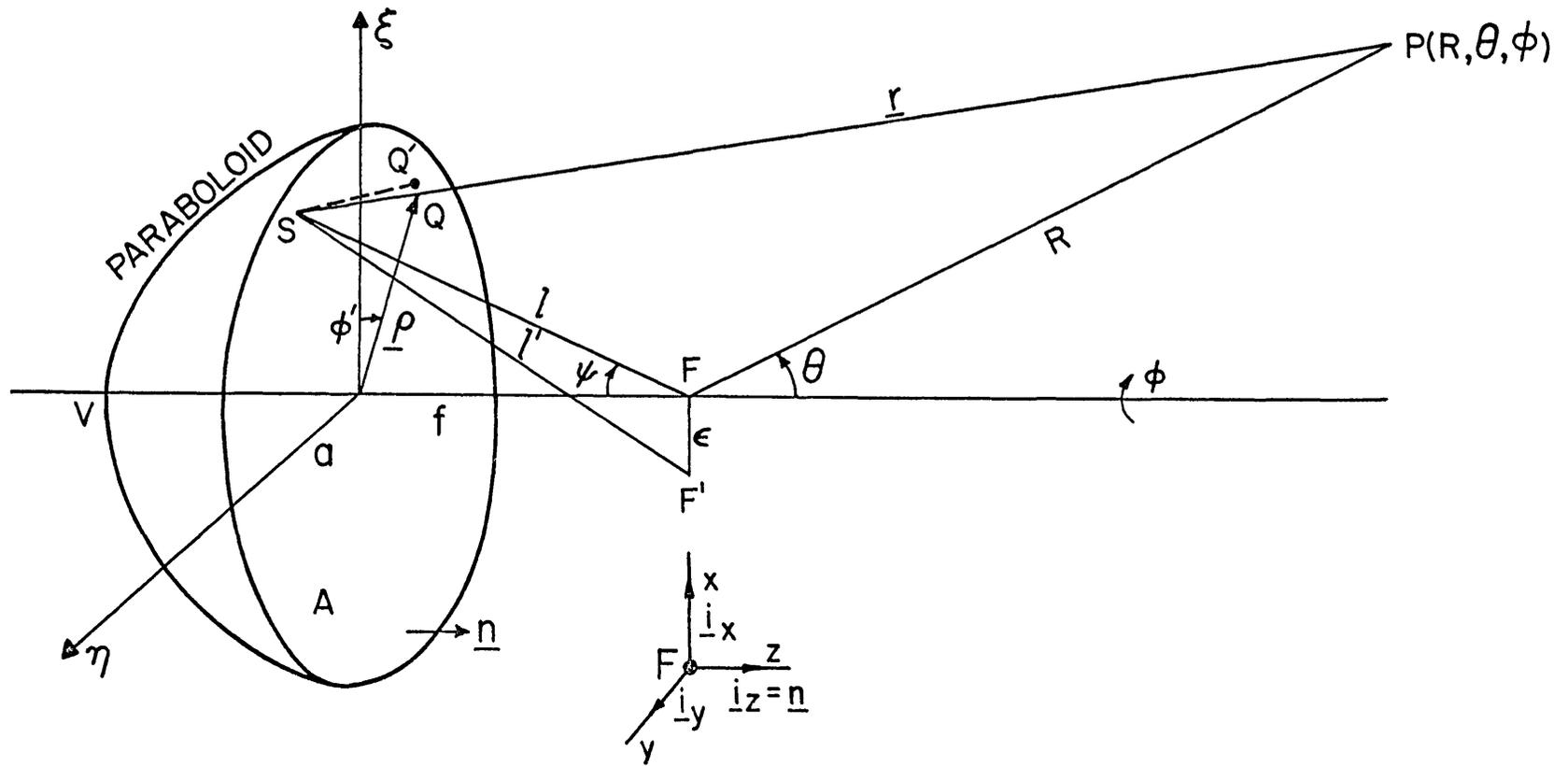
Figure 1 — Geometry of the Radiation Problem from a Circular Aperture
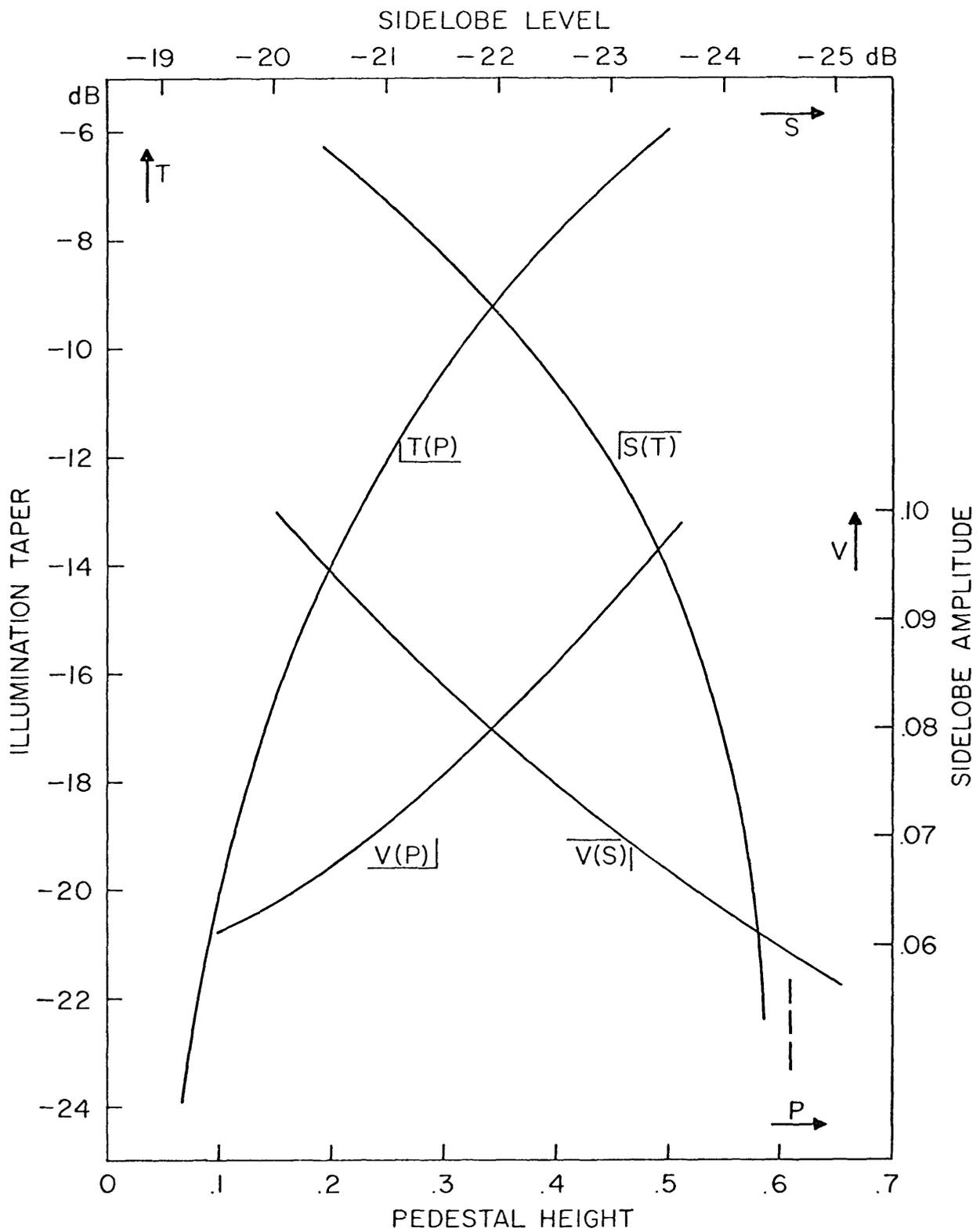
Figure 2 — Relationship Between the Taper T in dB, the Sidelobe Amplitude V,
Sidelobe Level S in dB and Pedestal Height p.
The two bars at rectangles around the curve designation indicate
the two coordinate axes pertaining to the curve.
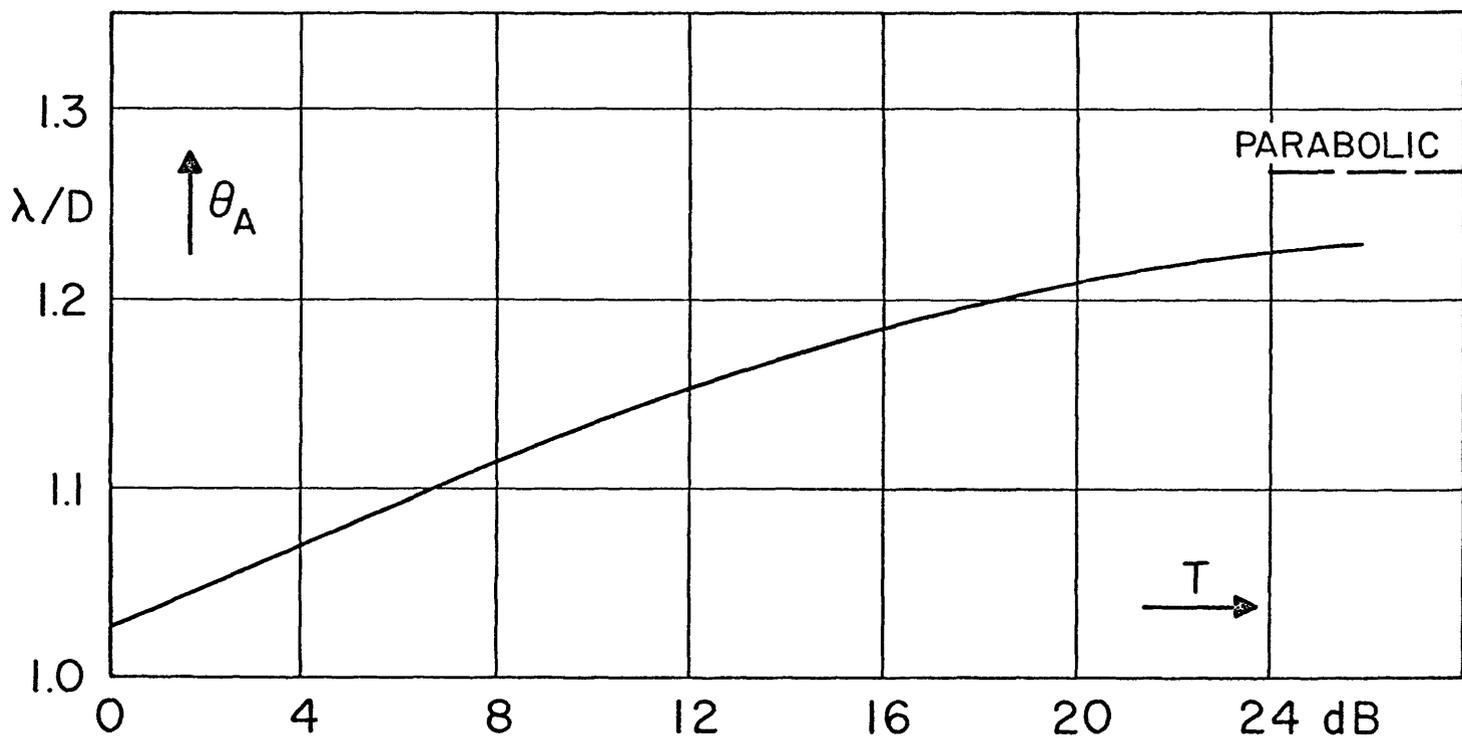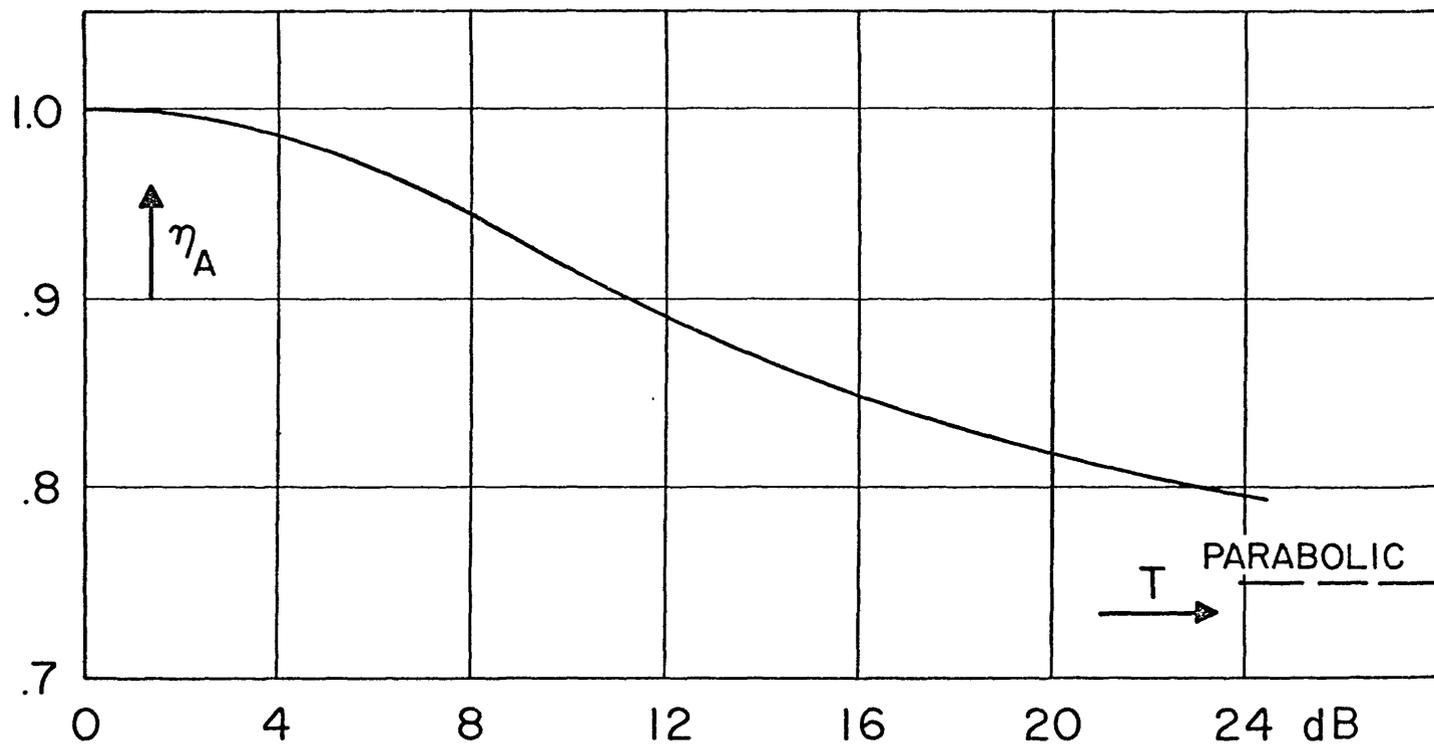
Figure 3 — Aperture Efficiency η_A and HPBW as Function of the Illumination Taper T.
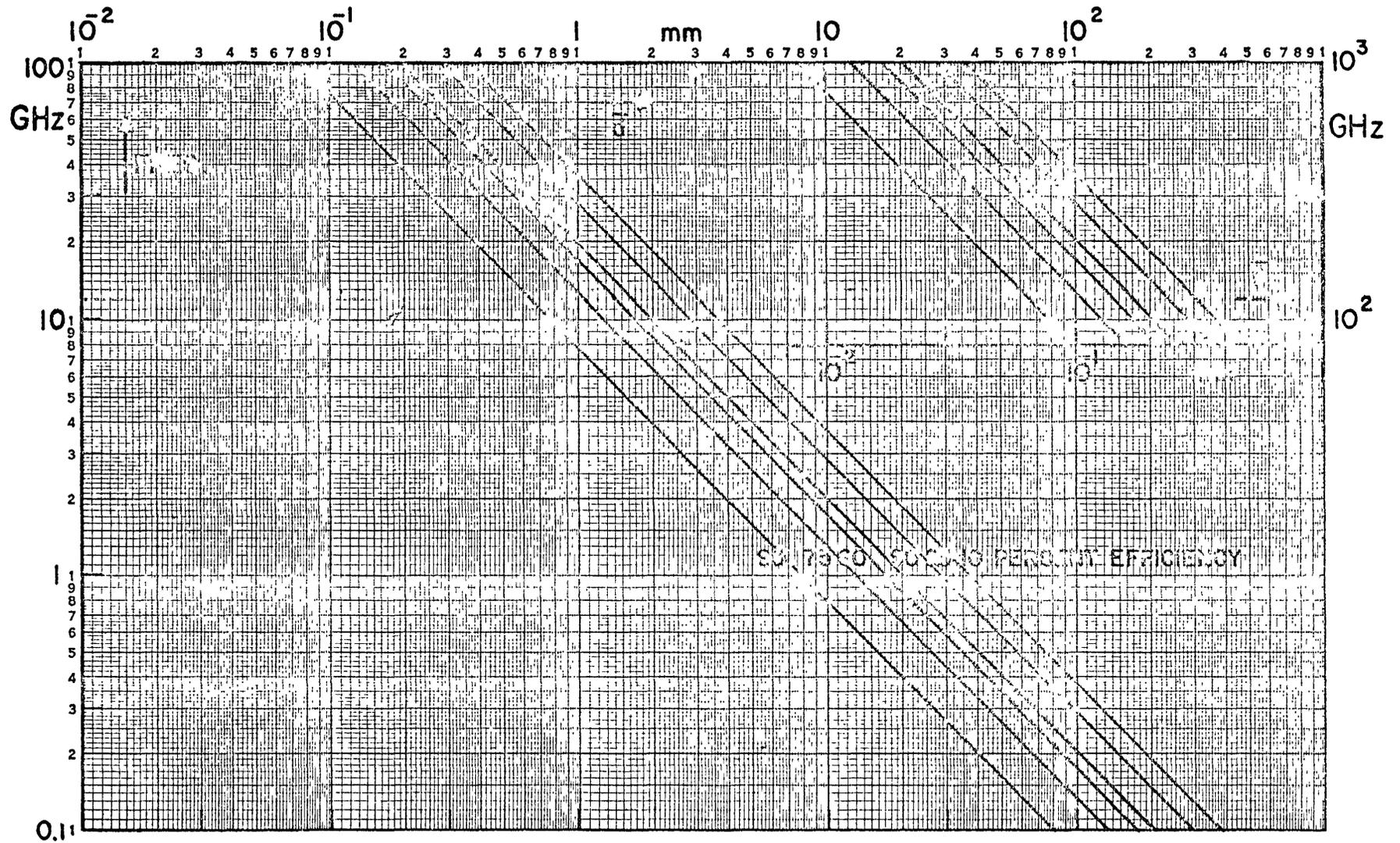
Figure 4 — Relative Decrease in Aperture Efficiency as Function of Random Surface Error $\bar{d}$ and Wavelength.
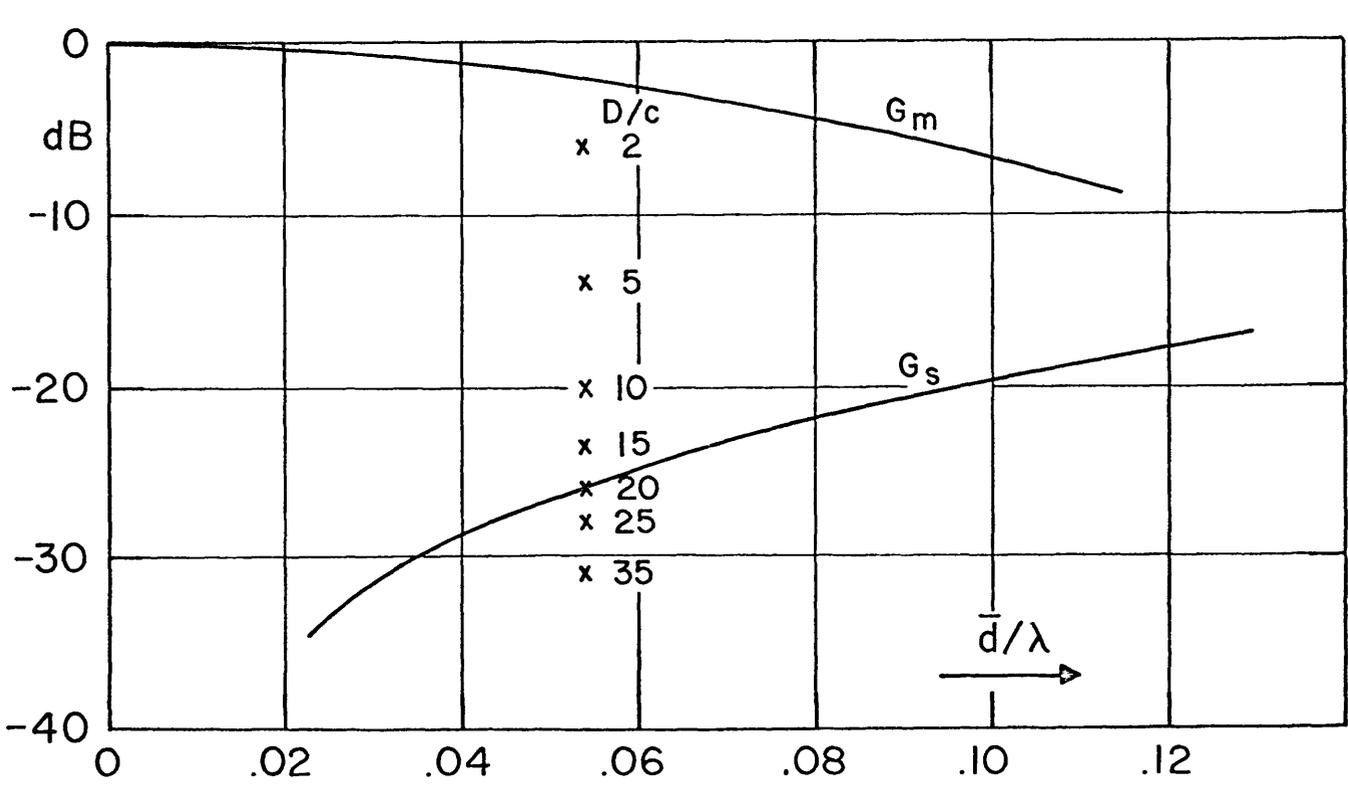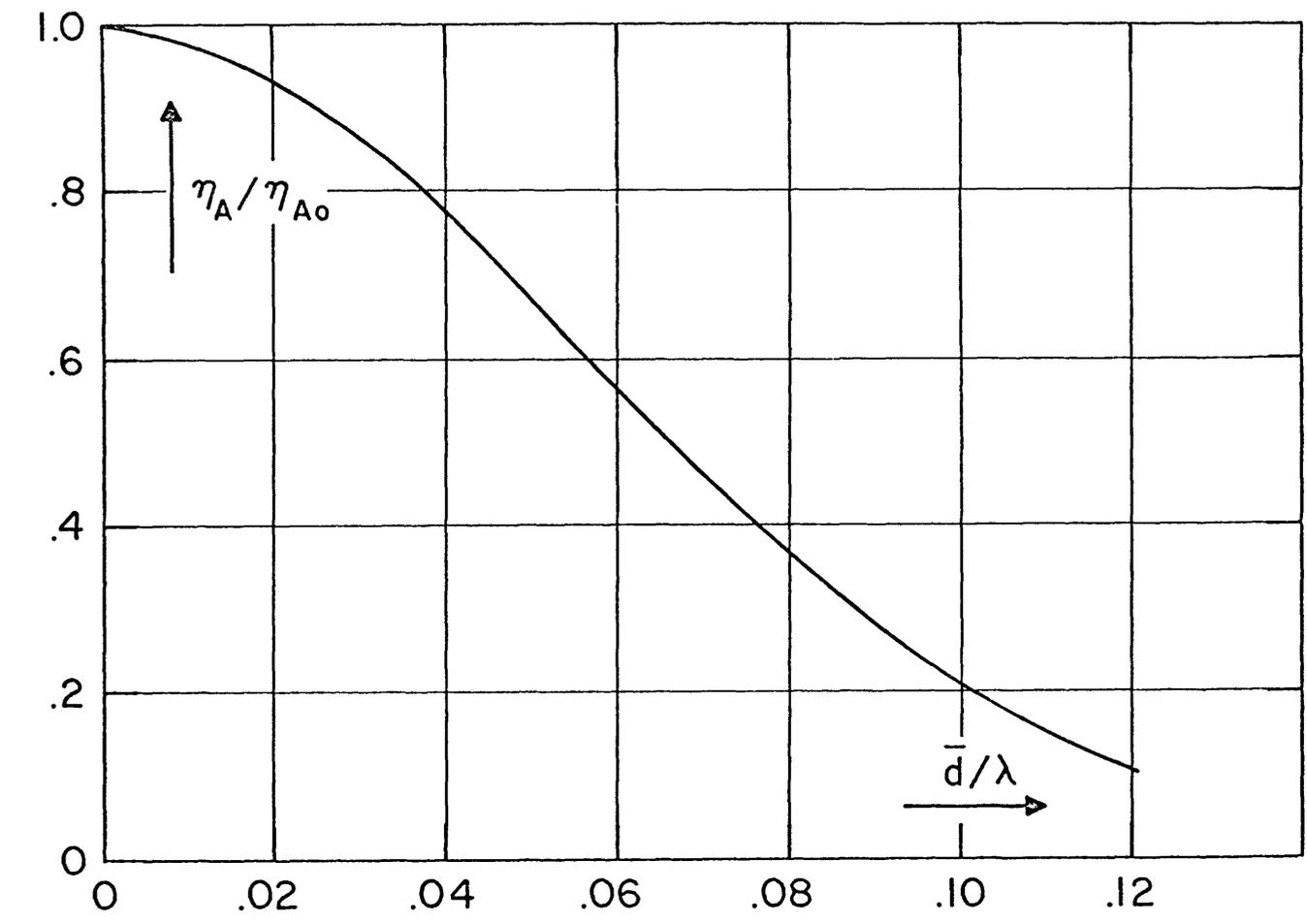
Figure 5 — Aperture Efficiency and Scatter Pattern Level as
Function of the Random Surface Error.
The correlation length C is parameter.
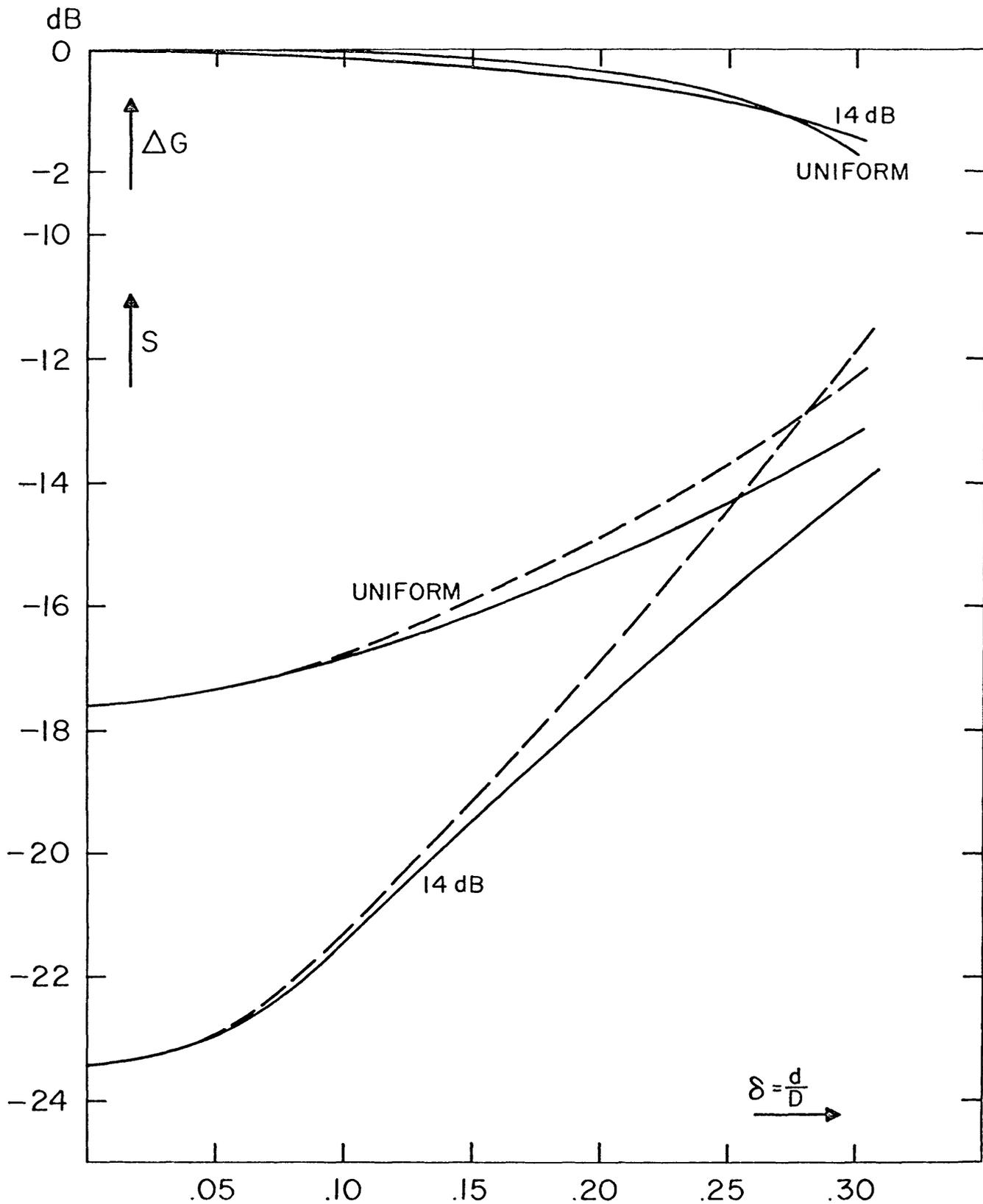
Figure 6 — The Gain Decrease ΔG and the Sidelobe Level S in dB as Function
of the Blocking Parameter δ.
Taper is parameter.
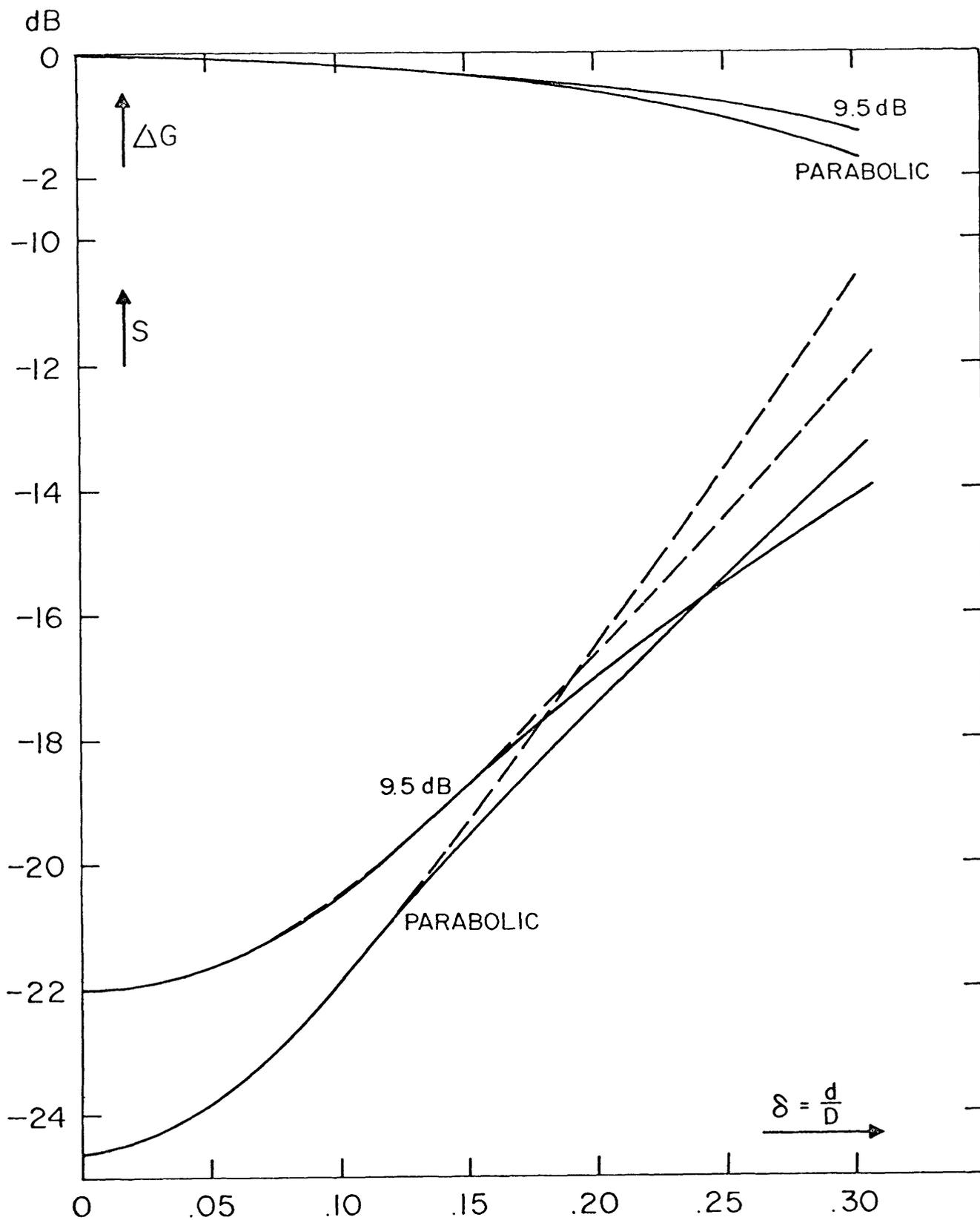
Figure 7 — The Gain Decrease ΔG and the Sidelobe Level S in dB as Function
of the Blocking Parameter δ.
Taper is parameter.
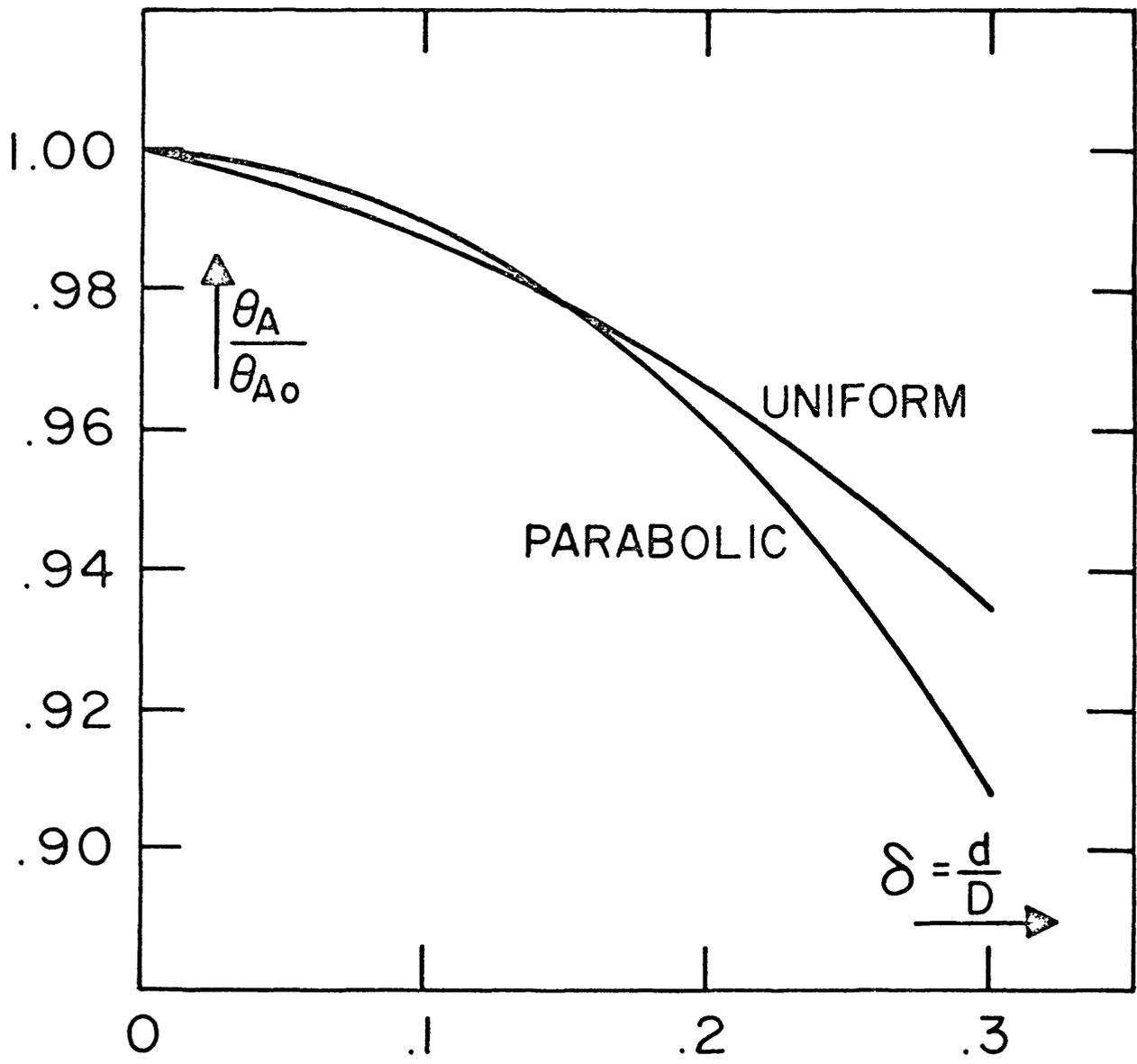
Figure 8 — The Relative Decrease in HPBW as Function of the Blocking
Parameter δ for Uniform and Parabolic Illumination.
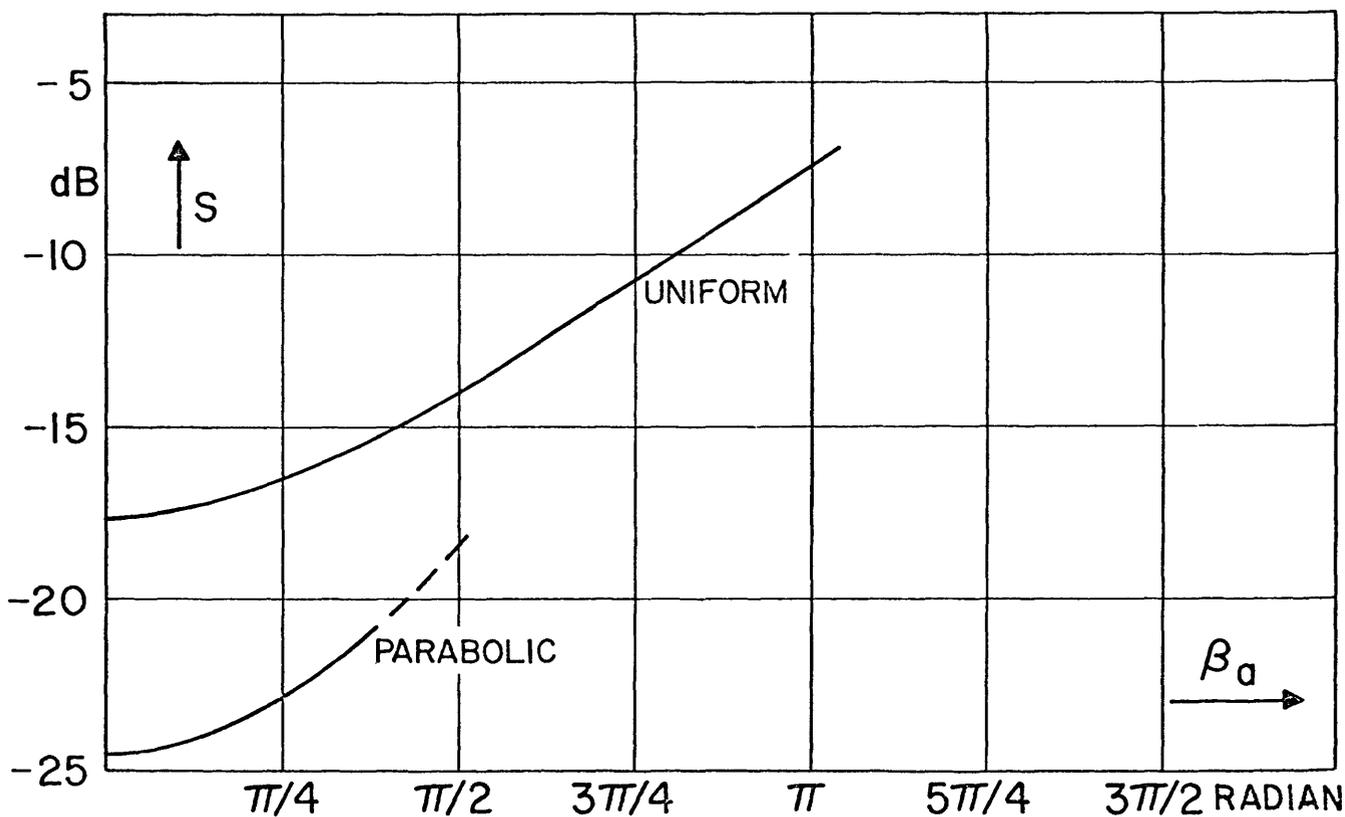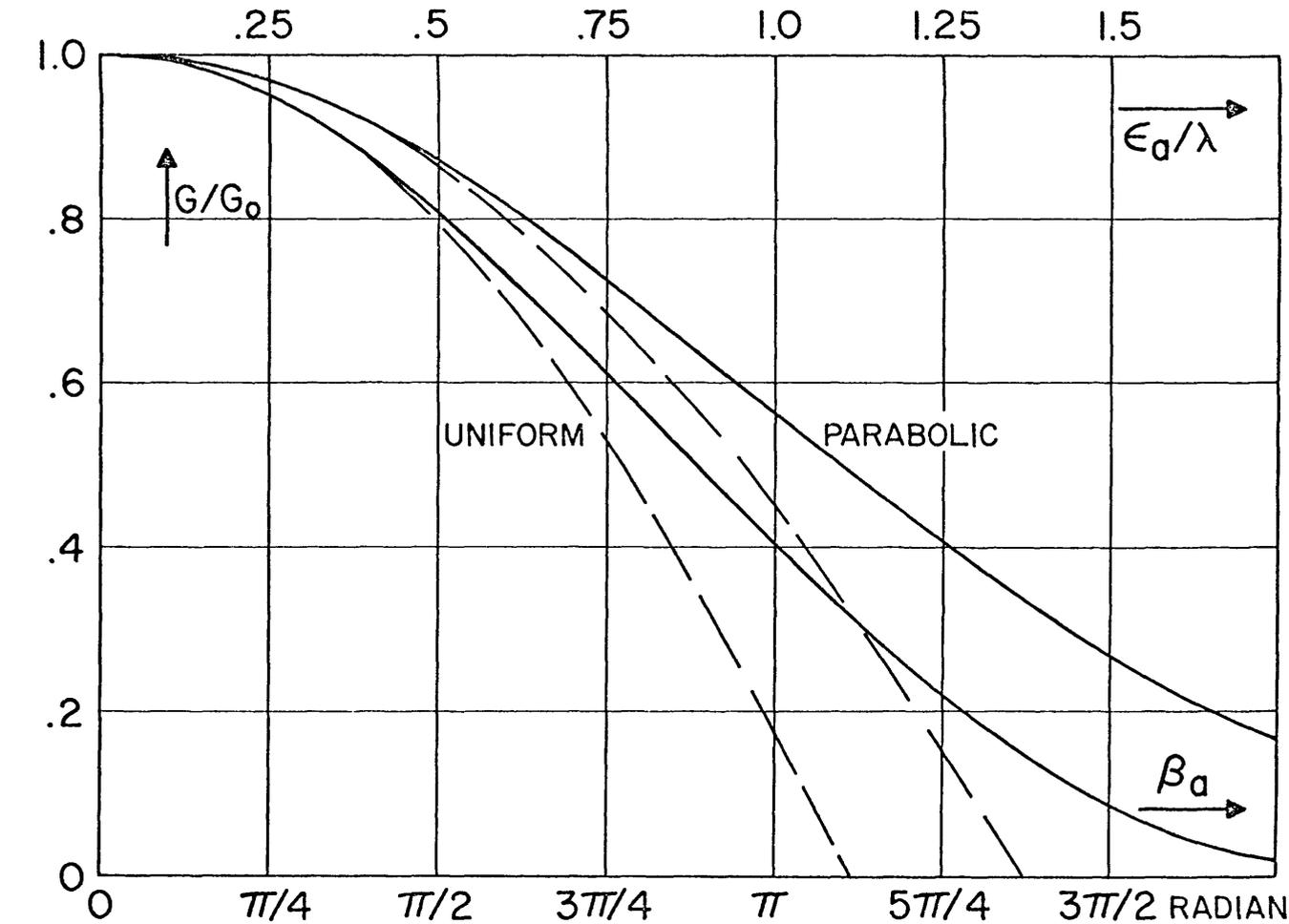
Figure 9 — Apperture Efficiency η_A and Sidelobe Level S as Function of the Maximum Phase Error β_a Over the Aperture Caused by a Feed Displacement ϵ_a Along the Antenna Axis (Axial Defocusing).

The top scale gives the defocusing in wavelengths and is applicable to antennas with 60° aperture angle (F/D = 0.42). The dashed curves are the quadratic approximations of equations (16) and (17).
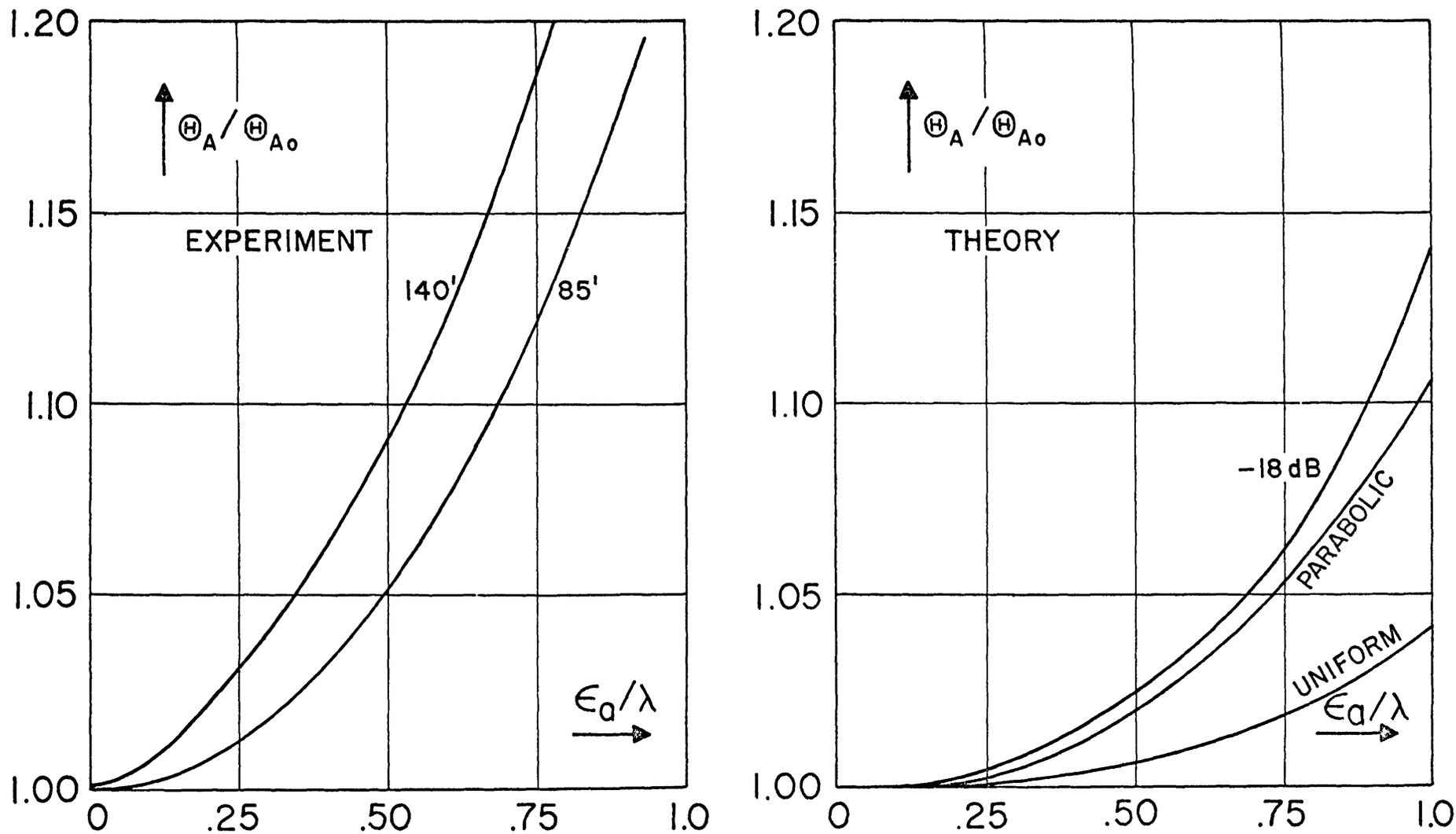
Figure 10 — Relative Beam Broadening as Function of Axial Defocusing.
The left hand curves are experimental results obtained at
2 cm wavelength on the 85-foot and 140-foot antennas. The
right hand curves are the result of theoretical calculations
for three illumination functions.
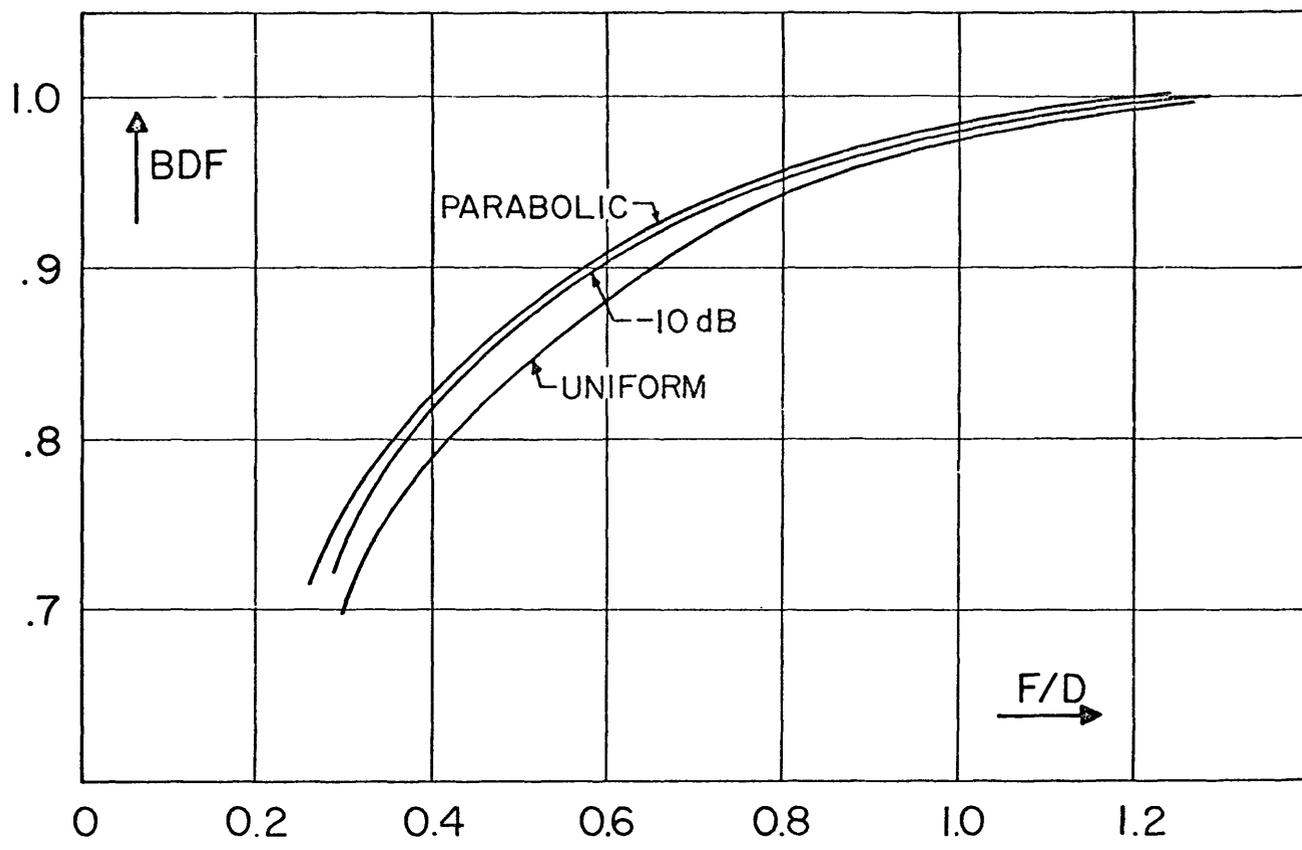
Figure 11 — The Beam Deviation Factor (BDF) as Function of the F/D Ratio.
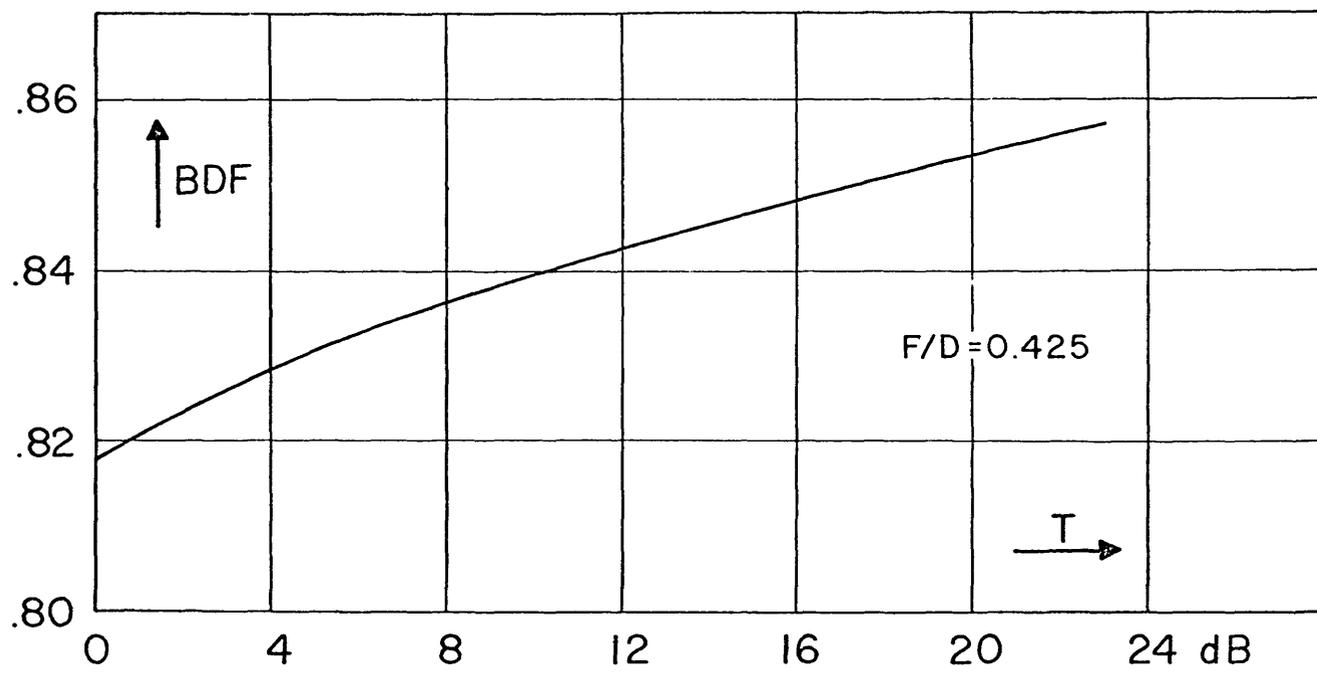The illumination taper is parameter.

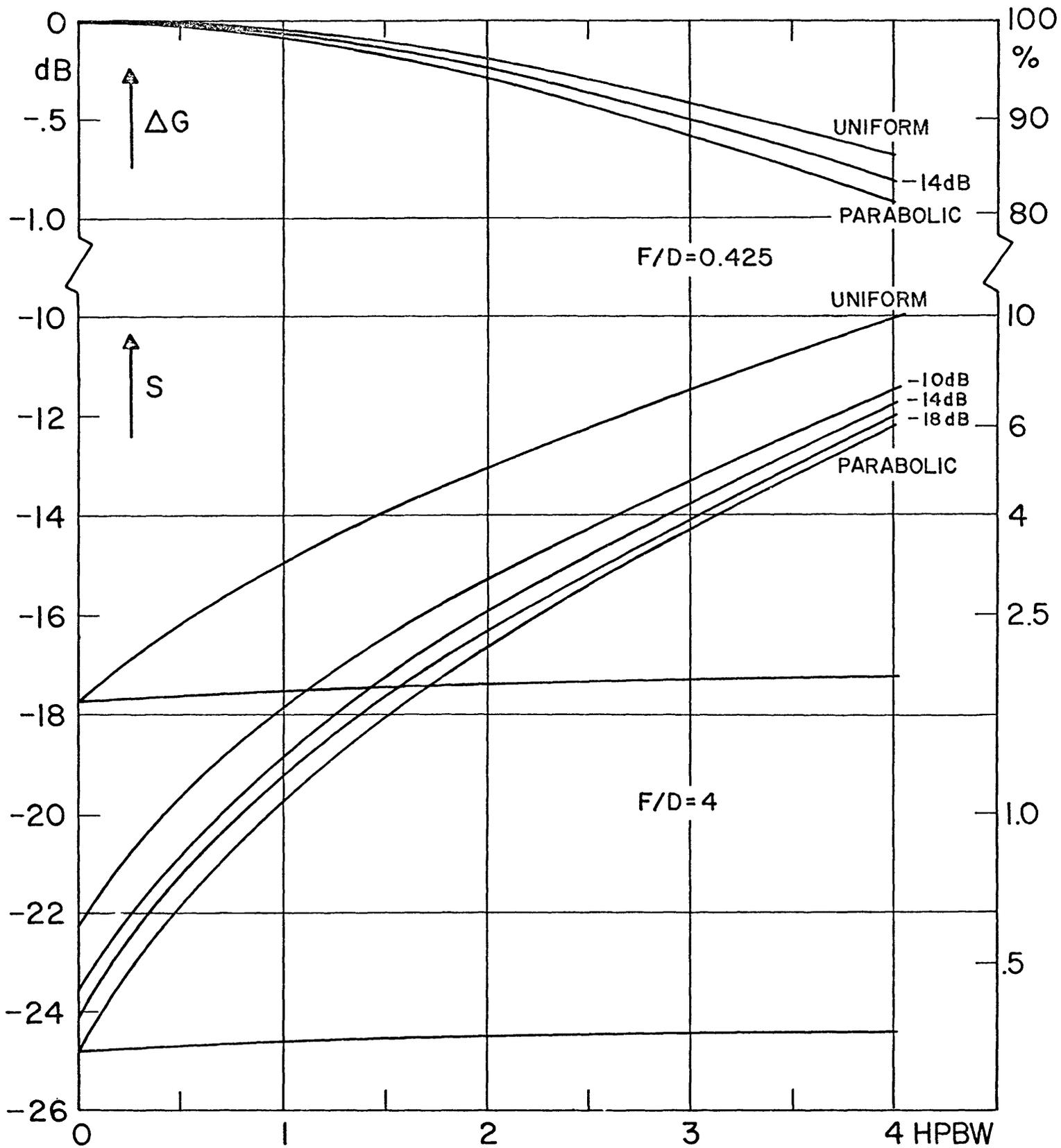Figure 12 — The BDF as Function of Illumination Taper for F/D = 0.425.

Figure 13 — Gain Loss ΔG and Sidelobe Level S (Coma Lobe) as Function
of Beam Tilt in HPBW Caused by Lateral Defocusing.
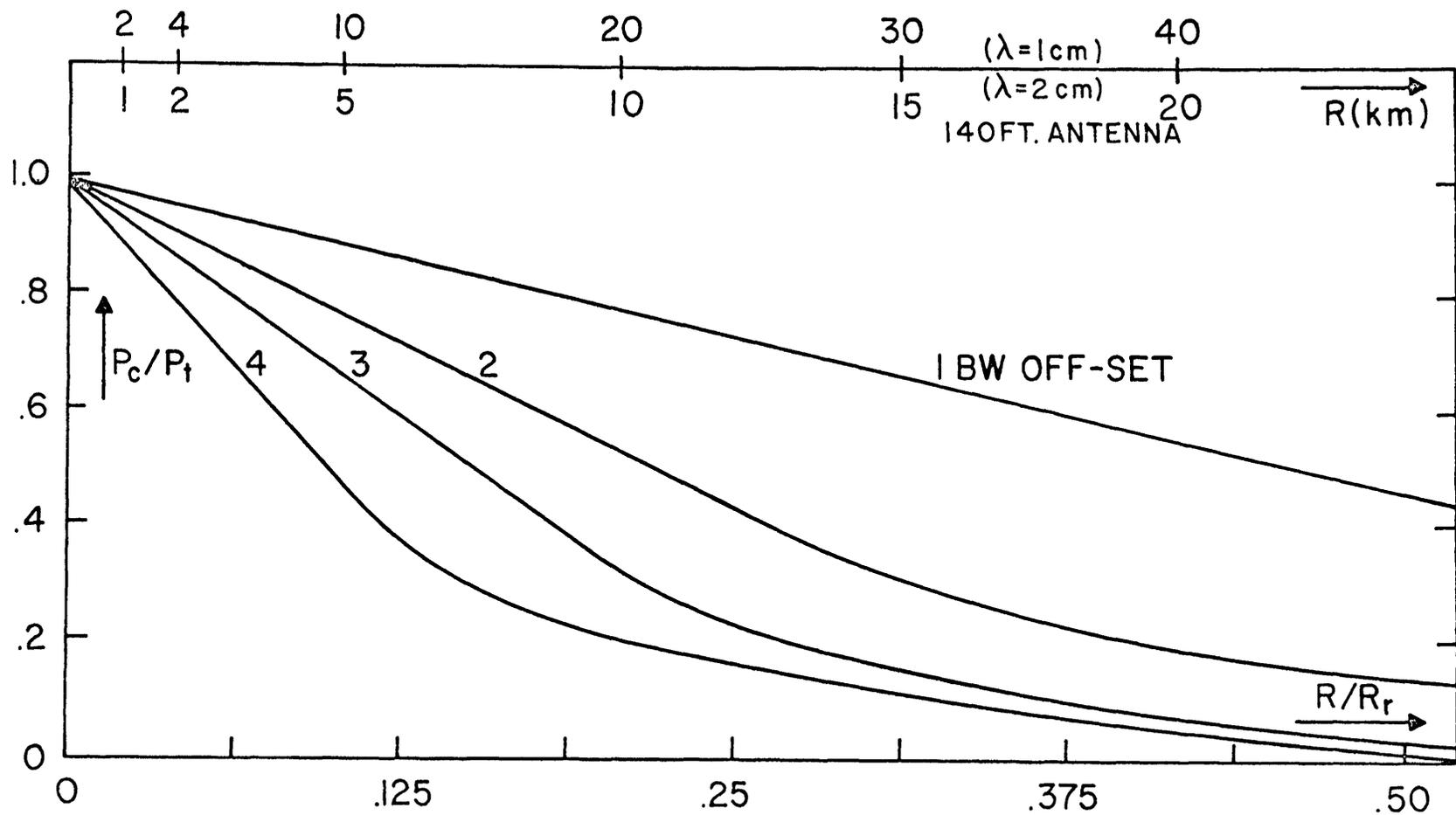The illumination taper is parameter. Also coma lobe for
F/D = 4 Cassegrain.

Figure 14 — Percentage of Common Power P_c/P_t in Two Partially Overlapping Beams as Function of the Distance Normalized to the Rayleigh Distance R_r to the Aperture. The beam separation in the farfield is parameter.
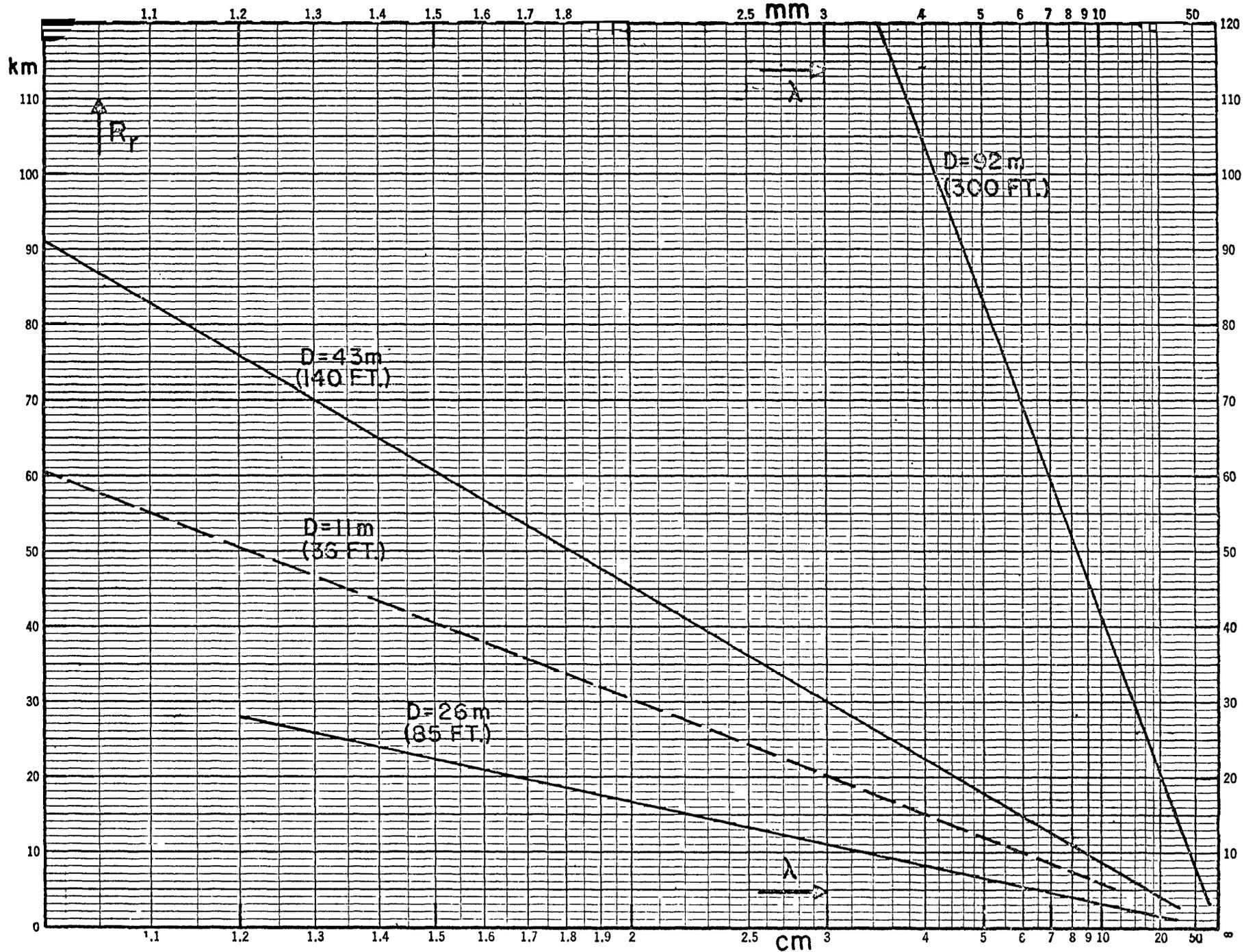
Figure 15 — The Rayleigh Distance $R_r = D^2/2\lambda$ as Function of the Wavelength for Several Antenna Diameters.
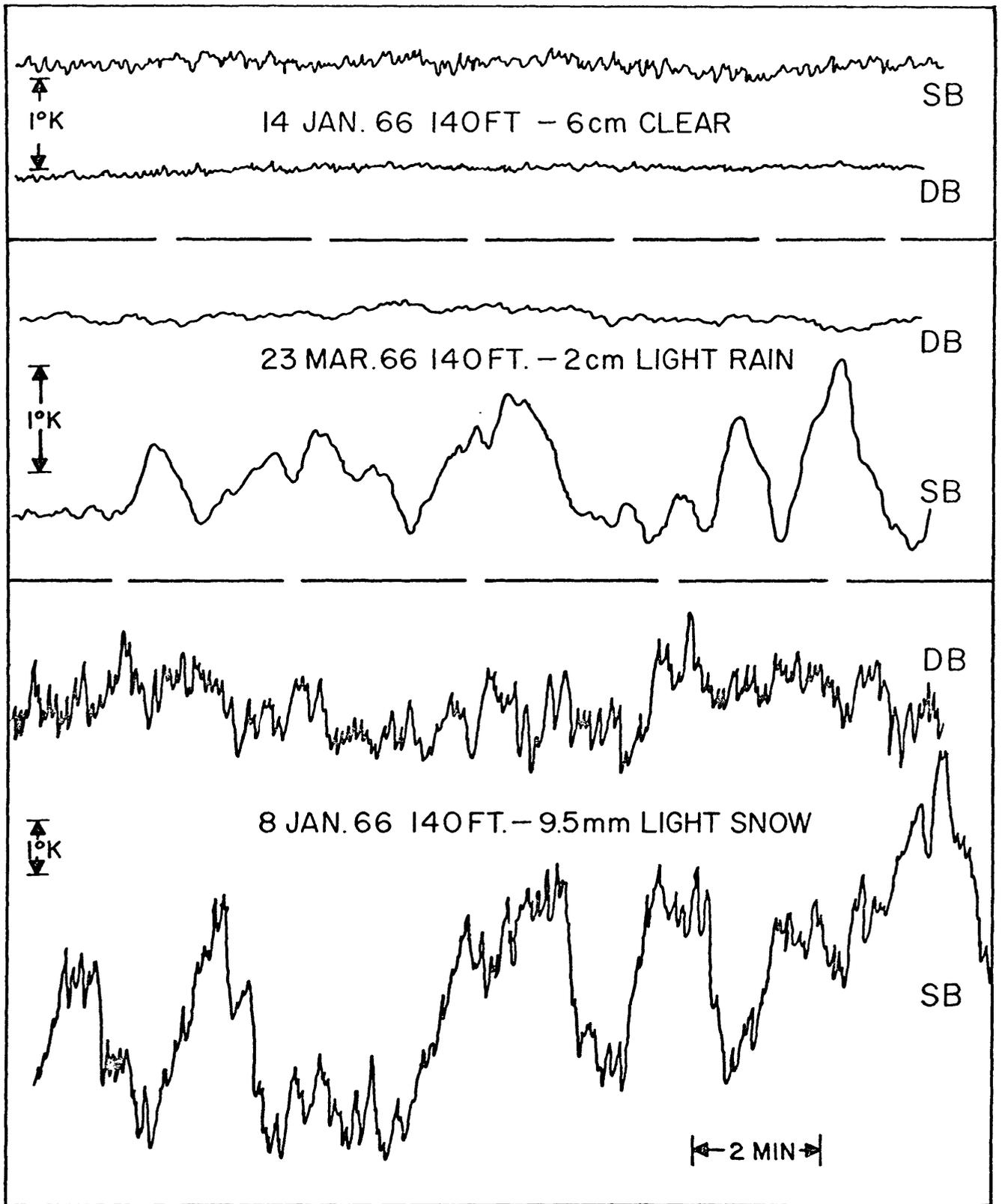
Figure 16 — Examples of Atmospheric Noise Observed at Several Wavelengths and Under Different Weather Conditions with the Single Beam (SB) and Dual Beam (DB) Mode. The vertical scale is in degrees antenna temperature.